

# Hybrid controlled-SUM gate with one superconducting qutrit and one cat-state qutrit and application in hybrid entangled state preparation

Qi-Ping Su<sup>1</sup>, Yu Zhang<sup>2</sup>, Liang Bin<sup>1</sup>, and Chui-Ping Yang<sup>1,3\*</sup>

<sup>1</sup>*School of Physics, Hangzhou Normal University, Hangzhou 311121, China*

<sup>2</sup>*School of Physics, Nanjing University, Nanjing 210093, China and*

<sup>3</sup>*Quantum Information Research Center, Shangrao Normal University, Shangrao 334001, China*  
(Dated: August 30, 2022)

Compared with a qubit, a qudit (i.e.,  $d$ -level or  $d$ -state quantum system) provides a larger Hilbert space to store and process information. On the other hand, qudit-based hybrid quantum computing usually requires performing hybrid quantum gates with qudits different in their nature or in their encoding format. In this work, we consider the qutrit case, i.e., the case for a qudit with  $d=3$ . We propose a simple method to realize a hybrid quantum controlled-SUM gate with one superconducting (SC) qutrit and a cat-state qutrit. This gate plus single-qutrit gates form a *universal* set of ternary logic gates for quantum computing with qutrits. Our proposal is based on circuit QED and operates essentially by employing a SC ququart (a four-level quantum system) dispersively coupled to a microwave cavity. The gate implementation is quite simple because it only requires a single basic operation. Neither classical pulse nor measurement is needed. The auxiliary higher energy level of the SC ququart is virtually excited during the gate operation, thus decoherence from this level is greatly suppressed. As an application of this gate, we discuss the generation of a hybrid maximally-entangled state of one SC qutrit and one cat-state qutrit. We further analyze the experimental feasibility of creating such hybrid entangled state in circuit QED. This proposal is quite general and can be extended to accomplish the same task in a wide range of physical system, such as a four-level natural or artificial atom coupled to an optical or microwave cavity.

PACS numbers: 03.67.Bg, 42.50.Dv, 85.25.Cp

## I. INTRODUCTION AND MOTIVATION

Quantum computers are in principle able to solve hard computational problems much more efficiently than classical computers [1-3]. In the past years, significant progress has been made in the implementation of quantum computers, where quantum information is either carried or stored using qubits, namely two-level or two-state quantum systems. On the other hand, qudits ( $d$ -level or  $d$ -state systems with  $d > 2$ ), instead of qubits, are used to perform quantum computing, which is now a developing field and has attracted growing attention. Because of its multi-level or multi-state nature, a qudit has a larger Hilbert space than a qubit. Thus, compared to their qubit-based counterparts, qudit-based processors can store exponentially greater information, implement certain algorithms using fewer entangling gates, and perform more powerful quantum computing [4-8]. Various physical platforms, such as photonic systems [9,10], ion trap [11], continuous spin systems [12,13], nitrogen-vacancy centers [14], nuclear magnetic resonance [6,15], molecular magnets [16], and superconducting circuits [17-21], have been applied to implement the qudit-based quantum computing.

Particularly, qutrits (three-level or three-state quantum systems) or qudits with  $d = 3$  have been studied both experimentally and theoretically. They can, in theory, be used for quantum error correction using small code size [22,23], quantum cryptography [24,25], and efficient communication protocols [26]. Experimentally, qutrits have been employed for fundamental tests of quantum mechanics [27] and used as auxiliary systems to accomplish various quantum computing tasks, such as implementing Toffoli gates [28] and multiqubit controlled-phase gates [29]. Moreover, quantum teleportations based on qutrits have been performed in photonic platforms [30,31]. As relevant to this work, experiments have demonstrated coherent population transfer in a superconducting qutrit [32], creation of GHZ entangled states of superconducting qutrits [20,21], and realization of single-qutrit quantum gates and a two-qutrit controlled-SUM (CSUM) gate with superconducting qutrits [18-20].

On the other hand, hybrid gates have attracted tremendous attention recently, because of their importance in connecting quantum information processors with different encoding information-processing units, as well as their

---

\*Electronic address: yangcp@hznu.edu.cn

significant application in transferring quantum states between a quantum processor and a quantum memory. A number of works on implementing hybrid gates with various qubits, qutrits or qudits have been presented (e.g., [33-43]). However, after a deep search of literature, we note that how to implement hybrid quantum gates with SC qutrits and cat-state qutrits (i.e., qutrits encoded via cat states) has not been studied yet.

In the following, we will propose a simple method to realize a hybrid quantum controlled-SUM (CSUM) gate with a three-level SC qutrit and a cat-state qutrit, based on circuit QED. The circuit QED, composed of microwave cavities and SC qubits or qudits, has appeared as one of the most promising candidates for quantum computing [44-51]. SC qubits or qudits, such as charge, flux, phase, transmon, and Xmon, can be fabricated using modern integrated circuit technology, their properties can be characterized and adjusted in situ, they have relatively long decoherence times [52-55], and thus they are good information processing units in quantum computing. In addition, the cat-state encoding, consisting of superpositions of coherent states, is protected against photon loss and dephasing errors [56,57], and quantum computing based on cat-state encoding has attracted much attention recently [58-60].

This proposal operates essentially by employing a SC ququart dispersively coupled to a microwave cavity. Here, “ququart” refers to a four-level quantum system, with three levels representing a qutrit and the fourth level acting as an auxiliary level for the state manipulation. The gate realization is quite simple because it only requires a single basic operation. As an application of this gate, we discuss the generation of a hybrid maximally-entangled state of a SC qutrit and a cat-state qutrit. We further analyze the circuit-QED experimental feasibility of creating such hybrid entangled state. This proposal is quite general and can be extended to accomplish the same task in a wide range of physical system, such as a four-level natural or artificial atom coupled to an optical or microwave cavity.

Other motivations of this work are as follows. First, hybrid gates of SC qutrits and cat-state qutrits are of significance in realizing a large-scale quantum computing executed in a compounded information processor, which is composed of a SC-qutrit based quantum processor and a cat-state-qutrit based quantum processor. Second, they are also important in the transmission of quantum states between a SC-qutrit based quantum processor and a cat-state-qutrit based quantum memory [61]. Cat-state qutrits could be good memory units for storing high-dimensional quantum states because experiments have demonstrated that the lifetime of storing quantum information via cat-state encoding can be greatly enhanced through quantum error correction [62]. Last, a two-qutrit CSUM gate plus single-qutrit gates form a *universal* set of ternary logic gates for quantum computing with qutrits [63-65], and thus implementing a hybrid two-qutrit CSUM gate becomes necessary in hybrid quantum computing with qutrits.

This paper is organized as follows. In Sec. II, we briefly introduce a hybrid two-qutrit CSUM gate. In Sec. III, we explicitly show how to realize this hybrid gate with a SC qutrit and a cat-state qutrit. In Sec. IV, we show how to generate a hybrid maximally-entangled state of a SC qutrit and a cat-state qutrit by applying this gate. In Sec. V, we give a discussion on the experimental feasibility of creating this hybrid entangled state, by employing a SC flux ququart coupled to a three-dimensional (3D) microwave cavity. A concluding summary is given in Sec. VI.

## II. HYBRID TWO-QUTRIT CSUM GATE

A qutrit has three logic states, which are denoted as  $|0\rangle$ ,  $|1\rangle$ , and  $|2\rangle$ , respectively. For two qutrits, there are a total number of nine computational basis states, i.e.,  $|00\rangle, |01\rangle, |02\rangle, |10\rangle, |11\rangle, |12\rangle, |20\rangle, |21\rangle$ , and  $|22\rangle$ . A two-qutrit CSUM gate is described by

$$\begin{aligned} |00\rangle &\rightarrow |00\rangle, & |01\rangle &\rightarrow |01\rangle, & |02\rangle &\rightarrow |02\rangle, \\ |10\rangle &\rightarrow |11\rangle, & |11\rangle &\rightarrow |12\rangle, & |12\rangle &\rightarrow |10\rangle, \\ |20\rangle &\rightarrow |22\rangle, & |21\rangle &\rightarrow |20\rangle, & |22\rangle &\rightarrow |21\rangle, \end{aligned} \quad (1)$$

which implies that: (i) if the control qutrit (the first qutrit) is in the state  $|1\rangle$ , the state  $|k\rangle$  of the target qutrit (the second qutrit) is shifted to the state  $|k \oplus 1\rangle$ ; (ii) if the control qutrit (the first qutrit) is in the state  $|2\rangle$ , the state  $|k\rangle$  of the target qutrit is shifted to the state  $|k \oplus 2\rangle$ ; however (iii) when the control qutrit is in the state  $|0\rangle$ , the state  $|k\rangle$  of the target qutrit remains unchanged. Here,  $k \in \{0, 1, 2\}$ ,  $|k \oplus 1\rangle$  means  $k + 1 \bmod 3$ , while  $|k \oplus 2\rangle$  represents  $k + 2 \bmod 3$ .

The hybrid two-qutrit CSUM gate considered in this work is described by Eq. (1). The control qutrit is a SC qutrit, whose three logic states are represented by the three lowest levels  $|0\rangle$ ,  $|1\rangle$ , and  $|2\rangle$  of a SC ququart (Fig. 1a), while the target qutrit is a cat-state qutrit, for which the three logic states  $|0\rangle$ ,  $|1\rangle$ , and  $|2\rangle$  are encoded via three quasi-orthogonal cat states of a cavity, which are given below

$$\begin{aligned} |0\rangle &= \mathcal{M}_0 (|\alpha\rangle + |-\alpha\rangle), \\ |1\rangle &= \mathcal{M}_1 (|\alpha e^{i\pi/3}\rangle + |-\alpha e^{i\pi/3}\rangle), \\ |2\rangle &= \mathcal{M}_2 (|\alpha e^{i2\pi/3}\rangle + |-\alpha e^{i2\pi/3}\rangle). \end{aligned} \quad (2)$$

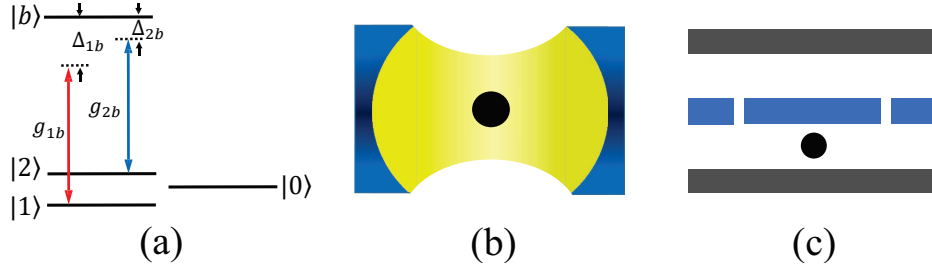


FIG. 1: (color online) (a) The cavity is dispersively coupled to the  $|1\rangle \leftrightarrow |b\rangle$  transition of the SC ququart with coupling constant  $g_{1b}$  and detuning  $\Delta_{1b}$ , while dispersively coupled to the  $|2\rangle \leftrightarrow |b\rangle$  transition of the SC ququart with coupling constant  $g_{2b}$  and detuning  $\Delta_{2b}$ . (b) Setup for one SC ququart embedded in a 3D microwave cavity. (c) Setup for a SC ququart coupled to a 1D microwave cavity or resonator. In (b) and (c), the dark dot represents the SC ququart.

Here,  $\mathcal{M}_0$ ,  $\mathcal{M}_1$ , and  $\mathcal{M}_2$  are normalization coefficients, with  $\mathcal{M}_0 = \mathcal{M}_1 = \mathcal{M}_2 = 1/\sqrt{2(1 + e^{-2|\alpha|^2})}$ . For  $\alpha \geq 3.05$ , one can verify  $|\langle k|l\rangle|^2 < 10^{-4}$  for  $k \neq l$  ( $k, l \in \{0, 1, 2\}$ ). Thus, when  $\alpha$  is large enough, any two of the three logic states of the cat-state qutrit can be made to be quasi-orthogonal to each other.

In the next section, we will show how to realize this hybrid CSUM gate. To avoid the confusion, please keep in mind that for each one of the states  $|00\rangle, |01\rangle, |02\rangle, |10\rangle, |11\rangle, |12\rangle, |20\rangle, |21\rangle$ , and  $|22\rangle$  listed below, the left 0, 1, and 2 correspond to the SC qutrit, while the right 0, 1, and 2 correspond to the cat-state qutrit.

### III. IMPLEMENTING A HYBRID TWO-QUTRIT CSUM GATE

Let us now consider a setup consisting of a microwave cavity and a SC ququart (Figs. 1b and 1c). The SC ququart has three lowest levels  $|0\rangle, |1\rangle, |2\rangle$  and an auxiliary higher-energy level  $|b\rangle$  (Fig. 1a). The SC ququart is initially decoupled from the cavity. The procedure for implementing the gate is listed below:

Adjust the cavity frequency such that the cavity is dispersively coupled to the  $|1\rangle \leftrightarrow |b\rangle$  transition of the SC ququart with coupling constant  $g_{1b}$  and detuning  $\Delta_{1b}$ , the cavity is dispersively coupled to the  $|2\rangle \leftrightarrow |b\rangle$  transition of the SC ququart with coupling constant  $g_{2b}$  and detuning  $\Delta_{2b}$ , but highly detuned (decoupled) from the transition between any other two levels of the SC ququart (Fig. 1a). Under these considerations, the Hamiltonian in the interaction picture is thus given by (in units of  $\hbar = 1$ )

$$H_I = g_{1b}(e^{i\Delta_{1b}t}\hat{a}|b\rangle\langle 1| + \text{h.c.}) + g_{2b}(e^{i\Delta_{2b}t}\hat{a}|b\rangle\langle 2| + \text{h.c.}), \quad (3)$$

where  $\hat{a}$  is the photon annihilation operator of the cavity,  $\Delta_{1b} = \omega_{1b} - \omega_c$ , and  $\Delta_{2b} = \omega_{2b} - \omega_c$ . Here,  $\omega_{1b}$  ( $\omega_{2b}$ ) is the  $|1\rangle \leftrightarrow |b\rangle$  ( $|2\rangle \leftrightarrow |b\rangle$ ) transition frequency of the ququart, while  $\omega_c$  is the cavity frequency.

In the large-detuning regime of  $|\Delta_{1b}| \gg g_{1b}$  and  $|\Delta_{2b}| \gg g_{2b}$ , the Hamiltonian (3) becomes [66-68]

$$H_e = -\lambda_1(\hat{a}^+\hat{a}|1\rangle\langle 1| - \hat{a}\hat{a}^+|b\rangle\langle b|) - \lambda_2(\hat{a}^+\hat{a}|2\rangle\langle 2| - \hat{a}\hat{a}^+|b\rangle\langle b|), \quad (4)$$

where  $\lambda_1 = g_{1b}^2/\Delta_{1b}$ ,  $\lambda_2 = g_{2b}^2/\Delta_{2b}$ , the terms in the first (second) bracket describe the photon-number dependent Stark shifts of the energy levels  $|1\rangle$  ( $|2\rangle$ ) and  $|b\rangle$ , which are induced by the cavity.

Note that the Hamiltonian (4) does not induce the transition between any two of the four levels  $|0\rangle, |1\rangle, |2\rangle$ , and  $|b\rangle$ . Hence, as long as the auxiliary level  $|b\rangle$  is initially unpopulated, this level will remain unoccupied. Therefore, the Hamiltonian (4) reduces to

$$\tilde{H}_e = -\lambda_1\hat{a}^+\hat{a}|1\rangle\langle 1| - \lambda_2\hat{a}^+\hat{a}|2\rangle\langle 2|. \quad (5)$$

For this Hamiltonian, the unitary operator  $U = e^{-i\tilde{H}_e t}$  results in the following state transformation

$$\begin{aligned} |10\rangle &\rightarrow |1\rangle \mathcal{M}_0 (|\alpha e^{i\lambda_1 t}\rangle + |-\alpha e^{i\lambda_1 t}\rangle), \\ |11\rangle &\rightarrow |1\rangle \mathcal{M}_1 (|\alpha e^{i\pi/3} e^{i\lambda_1 t}\rangle + |-\alpha e^{i\pi/3} e^{i\lambda_1 t}\rangle), \\ |12\rangle &\rightarrow |1\rangle \mathcal{M}_2 (|\alpha e^{i2\pi/3} e^{i\lambda_1 t}\rangle + |-\alpha e^{i2\pi/3} e^{i\lambda_1 t}\rangle), \\ |20\rangle &\rightarrow |2\rangle \mathcal{M}_0 (|\alpha e^{i\lambda_2 t}\rangle + |-\alpha e^{i\lambda_2 t}\rangle), \\ |21\rangle &\rightarrow |2\rangle \mathcal{M}_1 (|\alpha e^{i\pi/3} e^{i\lambda_2 t}\rangle + |-\alpha e^{i\pi/3} e^{i\lambda_2 t}\rangle), \\ |22\rangle &\rightarrow |2\rangle \mathcal{M}_2 (|\alpha e^{i2\pi/3} e^{i\lambda_2 t}\rangle + |-\alpha e^{i2\pi/3} e^{i\lambda_2 t}\rangle), \end{aligned} \quad (6)$$

where on the left side the three logic states  $|0\rangle$ ,  $|1\rangle$ , and  $|2\rangle$  of the cat-state qutrit are defined in Eq. (2) above..

If we set

$$\lambda_1 t = \pi/3, \quad \lambda_2 t = 2\pi/3, \quad (7)$$

(i.e.,  $\lambda_2 = 2\lambda_1$ ), then the state transformation (6) becomes

$$\begin{aligned} |10\rangle &\rightarrow |1\rangle \mathcal{M}_0 \left( |\alpha e^{i\pi/3}\rangle + |-\alpha e^{i\pi/3}\rangle \right), \\ |11\rangle &\rightarrow |1\rangle \mathcal{M}_1 \left( |\alpha e^{i2\pi/3}\rangle + |-\alpha e^{i2\pi/3}\rangle \right), \\ |12\rangle &\rightarrow |1\rangle \mathcal{M}_2 (|\alpha\rangle + |-\alpha\rangle), \\ |20\rangle &\rightarrow |2\rangle \mathcal{M}_0 \left( |\alpha e^{i2\pi/3}\rangle + |-\alpha e^{i2\pi/3}\rangle \right), \\ |21\rangle &\rightarrow |2\rangle \mathcal{M}_1 (|\alpha\rangle + |-\alpha\rangle), \\ |22\rangle &\rightarrow |2\rangle \mathcal{M}_2 \left( |\alpha e^{i\pi/3}\rangle + |-\alpha e^{i\pi/3}\rangle \right). \end{aligned} \quad (8)$$

According to the three logic states of the cat-state qutrit defined in Eq. (2) and because of  $\mathcal{M}_0 = \mathcal{M}_1 = \mathcal{M}_2$ , the state transformation (8) can be written as

$$\begin{aligned} |10\rangle &\rightarrow |11\rangle, \quad |11\rangle \rightarrow |12\rangle, \quad |12\rangle \rightarrow |10\rangle, \\ |20\rangle &\rightarrow |22\rangle, \quad |21\rangle \rightarrow |20\rangle, \quad |22\rangle \rightarrow |21\rangle. \end{aligned} \quad (9)$$

On the other hand, it is noted that the Hamiltonian (5) does not involve the level  $|0\rangle$  of the SC ququart, hence this Hamiltonian (5) acting on the three states  $|00\rangle$ ,  $|01\rangle$ , and  $|02\rangle$  results in zero, i.e.,  $\tilde{H}_e |00\rangle = \tilde{H}_e |01\rangle = \tilde{H}_e |02\rangle \equiv 0$ . As a result, the other three states  $|00\rangle$ ,  $|01\rangle$ ,  $|02\rangle$  of the two qutrits remain unchanged under the unitary operator  $U = e^{-i\tilde{H}_e t}$ , i.e.,

$$|00\rangle \rightarrow |00\rangle, \quad |01\rangle \rightarrow |01\rangle, \quad |02\rangle \rightarrow |02\rangle. \quad (10)$$

Therefore, it can be concluded from Eqs. (9) and (10) that the hybrid two-qutrit CSUM gate described by Eq. (1) is implemented with a SC qutrit (the control qutrit) and a cat-state qutrit (the target qutrit) after the above operation. It should be noted that after the operation, the cavity frequency needs to be adjusted back such that the cavity is decoupled from the SC ququart.

In the above, we have set  $\lambda_2 = 2\lambda_1$ , which turns out into

$$g_{2b}^2/\Delta_{2b} = 2g_{1b}^2/\Delta_{1b}. \quad (11)$$

Note that this condition (11) can be readily satisfied by carefully selecting  $g_{1b}$ ,  $g_{2b}$ ,  $\Delta_{1b}$  or  $\Delta_{2b}$ .

During the gate operation described above, the coupling or decoupling of the SC ququart with the cavity is realized by adjusting the cavity frequency. For a superconducting microwave cavity, the cavity frequency can be rapidly (within a few nanoseconds) tuned in experiments [69-71]. Alternatively, the coupling or decoupling of the SC ququart with the cavity can be obtained by adjusting the level spacings of the SC ququart. For superconducting qubits or qudits, their level spacings can be rapidly (within 1-3 ns) adjusted by varying external control parameters [72,73].

As shown above, the gate realization requires only a single basic operation described by  $U$ . During the gate operation, the auxiliary higher energy level  $|b\rangle$  of the ququart is virtually excited and thus decoherence from this level is greatly suppressed. Moreover, neither applying a classical pulse to the qutrit nor making measurement on the state of the SC ququart or the cavity is needed.

#### IV. PREPARING A HYBRID MAXIMALLY-ENTANGLED STATE OF TWO QUTRITS

Hybrid entangled states play a crucial role in quantum information processing and quantum technology. For instance, hybrid entangled states can be used as quantum channels and intermediate resources for quantum technology, including quantum information transmission, quantum state operation, and storage between different encodings and formats [74-76]. They can also act as practical interfaces to connect quantum processors with information processing units of different encoding. Generally speaking, hybrid entangled states involve subsystems different in their nature (e.g., photons and matters) or in the degree of freedom (e.g., discrete-variable degree and continuous variable degree).

Assume that the SC ququart is in a superposition state  $(|0\rangle + |1\rangle + |2\rangle)/\sqrt{3}$ , which can be easily prepared by applying resonant classical pulses to the SC ququart. Namely, apply a classical pulse (with an initial phase  $\phi = -\pi/2$ ,

a duration  $\tau = \Omega_1^{-1} \arccos 1/\sqrt{3}$ , resonant to the  $|0\rangle \leftrightarrow |1\rangle$  transition of the ququart in the state  $|0\rangle$ ) to achieve the state transformation  $|0\rangle \rightarrow 1/\sqrt{3}|0\rangle + \sqrt{2/3}|1\rangle$  [77]; then apply a second classical pulse (with an initial phase  $\phi = -\pi/2$ , a duration  $\tau = \Omega_2^{-1}\pi/4$ , resonant to the  $|1\rangle \leftrightarrow |2\rangle$  transition of the ququart) to achieve the state transformation  $|1\rangle \rightarrow (|1\rangle + |2\rangle)/\sqrt{2}$ . Here,  $\Omega_1$  ( $\Omega_2$ ) is the Rabi frequency of the first (second) pulse. It is easy to check that the superposition state  $(|0\rangle + |1\rangle + |2\rangle)/\sqrt{3}$  of the ququart is prepared by combination of these two state transformations.

Suppose that the cavity is in the cat state  $|0\rangle = \mathcal{M}_0(|\alpha\rangle + |-\alpha\rangle)$ . Note that this cat state has been experimentally created in circuit QED [78-82]. The initial state of the system is thus given by

$$|\psi(0)\rangle = \frac{1}{\sqrt{3}}(|0\rangle + |1\rangle + |2\rangle)|0\rangle. \quad (12)$$

Now we perform the operation described in the preceding section to achieve a hybrid two-qutrit CSUM gate (1). From Eq. (1), one can see that after this gate operation, the state (12) becomes

$$\frac{1}{\sqrt{3}}(|00\rangle + |11\rangle + |22\rangle), \quad (13)$$

which is the hybrid maximally-entangled state of a SC qutrit and a cat-state qutrit.

As can be seen from the above description, applying the hybrid two-qutrit CSUM gate (1) can directly create the hybrid maximally-entangled state (13) of a SC qutrit and a cat-state qutrit. Given that the initial state (12) of the system is ready, the operation time for preparing the hybrid entangled state (13) is equal to that for implementing the gate (1), i.e.,  $t = \pi/(3\lambda_1)$ . Since the hybrid entangled state here is created based on the gate (1), the Hamiltonian used for generating the hybrid entangled state (13) is the same as that used for realizing the gate (1).

#### IV. EXPERIMENTAL FEASIBILITY

As an example, let us now give a brief discussion on the possibility of experimentally creating the hybrid entangled state (13), by considering a setup of a SC flux ququart coupled to a 3D microwave cavity (Fig. 1b). The SC flux ququart has four levels as depicted in Fig. 2a, where the *ground* level is labelled by  $|1\rangle$ . Note that the transition between the level  $|0\rangle$  and any one of the other three levels  $\{|1\rangle, |2\rangle, |b\rangle\}$  can be made weak by increasing the barrier between the two potential wells.

As shown in the previous section, the hybrid entangled state (13) was created by applying the hybrid CSUM gate (1). In this sense, as long as the initial state (12) can be well prepared, the operational fidelity for the preparation of the hybrid entangled state (13) depends mainly on the performance of the hybrid CSUM gate (1) on a SC qutrit and a cat-state qutrit.

##### A. Full Hamiltonian

The hybrid CSUM gate (1) was implemented based on the effective Hamiltonian (5), which was derived starting from the original Hamiltonian (3). Note that the Hamiltonian (3) only contains the coupling of the cavity with the  $|1\rangle \leftrightarrow |b\rangle$  transition and the coupling of the cavity with the  $|2\rangle \leftrightarrow |b\rangle$  transition of the SC flux ququart. In reality, there exist the unwanted couplings of the cavity with other intra-level transitions of the SC flux ququart.

By taking the unwanted couplings into account, the Hamiltonian (3) is modified as (without RWA)

$$\begin{aligned} H'_1 = & g_{1b}(e^{i\Delta_{1b}t}\hat{a}|b\rangle\langle 1| + \text{h.c.}) + g_{1b} \left[ e^{i(\omega_c + \omega_{1b})t}\hat{a}^+|b\rangle\langle 1| + \text{h.c.} \right] \\ & + g_{2b}(e^{i\Delta_{2b}t}\hat{a}|b\rangle\langle 2| + \text{h.c.}) + g_{2b} \left[ e^{i(\omega_c + \omega_{2b})t}\hat{a}^+|b\rangle\langle 2| + \text{h.c.} \right] \\ & + g_{0b}(e^{i\Delta_{0b}t}\hat{a}|b\rangle\langle 0| + \text{h.c.}) + g_{0b} \left[ e^{i(\omega_c + \omega_{0b})t}\hat{a}^+|b\rangle\langle 0| + \text{h.c.} \right] \\ & + g_{01}(e^{i\Delta_{01}t}\hat{a}|0\rangle\langle 1| + \text{h.c.}) + g_{01} \left[ e^{i(\omega_c + \omega_{01})t}\hat{a}^+|0\rangle\langle 1| + \text{h.c.} \right] \\ & + g_{02}(e^{i\Delta_{02}t}\hat{a}|2\rangle\langle 0| + \text{h.c.}) + g_{02} \left[ e^{i(\omega_c + \omega_{02})t}\hat{a}^+|2\rangle\langle 0| + \text{h.c.} \right] \\ & + g_{12}(e^{i\Delta_{12}t}\hat{a}|2\rangle\langle 1| + \text{h.c.}) + g_{12} \left[ e^{i(\omega_c + \omega_{12})t}\hat{a}^+|2\rangle\langle 1| + \text{h.c.} \right], \end{aligned} \quad (14)$$

where the terms in the first line correspond to the coupling of the cavity with the  $|1\rangle \leftrightarrow |b\rangle$  transition of the SC ququart, the terms in the second line correspond to the coupling of the cavity with the  $|2\rangle \leftrightarrow |b\rangle$  transition of the SC ququart, the terms in the third line correspond to the unwanted coupling between the cavity and the  $|0\rangle \leftrightarrow |b\rangle$  transition of the SC ququart with coupling constant  $g_{0b}$ , the terms in the fourth line correspond to the unwanted

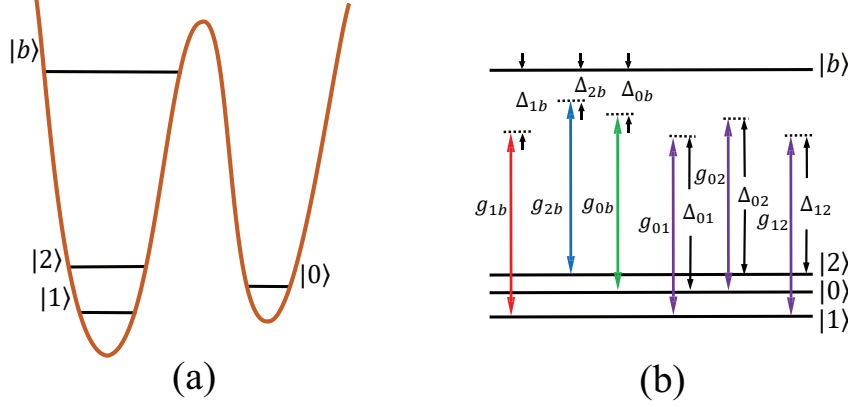


FIG. 2: (color online) (a) Illustration of the four levels of a SC flux ququart. Note that the *ground* level is labelled by  $|1\rangle$ . The transition between the level  $|0\rangle$  and any one of the other three levels  $\{|1\rangle, |2\rangle, |b\rangle\}$  is weak due to the barrier between the two potential wells. (b) Illustration of the cavity being dispersively coupled to the  $|k\rangle \leftrightarrow |b\rangle$  transition of the SC ququart with coupling constant  $g_{kb}$  and detuning  $\Delta_{kb}$  ( $k = 1, 2$ ), the unwanted coupling between the cavity and the  $|0\rangle \leftrightarrow |b\rangle$  transition of the SC ququart with coupling constant  $g_{0b}$  and detuning  $\Delta_{0b}$ , as well as the unwanted coupling between the cavity and the  $|m\rangle \leftrightarrow |n\rangle$  transition of the SC ququart with coupling constant  $g_{mn}$  and detuning  $\Delta_{mn}$  ( $mn = 01, 02, 12$ ).

coupling between the cavity and the  $|0\rangle \leftrightarrow |1\rangle$  transition of the SC ququart with coupling constant  $g_{01}$ , the terms in the fifth line correspond to the unwanted coupling between the cavity and the  $|0\rangle \leftrightarrow |2\rangle$  transition of the SC ququart with coupling constant  $g_{02}$ , and the terms in the last line correspond to the unwanted coupling between the cavity and the  $|1\rangle \leftrightarrow |2\rangle$  transition of the SC ququart with coupling constant  $g_{12}$  (Fig. 2b). In Eq. (14),  $\Delta_{0b}$ ,  $\Delta_{01}$ ,  $\Delta_{02}$ , and  $\Delta_{12}$  are detunings, which are given by  $\Delta_{0b} = \omega_{0b} - \omega_c$ ,  $\Delta_{01} = \omega_{01} - \omega_c$ ,  $\Delta_{02} = \omega_{02} - \omega_c$ , and  $\Delta_{12} = \omega_{12} - \omega_c$  (Fig. 2b). Here,  $\omega_{0b}$ ,  $\omega_{01}$ ,  $\omega_{02}$ , and  $\omega_{12}$  are the  $|0\rangle \leftrightarrow |b\rangle$ ,  $|0\rangle \leftrightarrow |1\rangle$ ,  $|0\rangle \leftrightarrow |2\rangle$ , and  $|1\rangle \leftrightarrow |2\rangle$  transition frequencies of the ququart, respectively.

## B. Numerical results

The dynamics of the lossy system, with ququart relaxation, dephasing and cavity decay being included, is determined by

$$\begin{aligned}
 \frac{d\rho}{dt} = & -i[H'_1, \rho] + \kappa\mathcal{L}[\hat{a}] \\
 & + \sum_{j=0,1,2} \gamma_{jb}\mathcal{L}[\sigma_{jb}^-] + \sum_{j=0,1} \gamma_{j2}\mathcal{L}[\sigma_{j2}^-] + \gamma_{01}\mathcal{L}[\sigma_{01}^-] \\
 & + \sum_{j=0,2,b} \gamma_{j,\varphi}(\sigma_{jj}\rho\sigma_{jj} - \sigma_{jj}\rho/2 - \rho\sigma_{jj}/2),
 \end{aligned} \tag{15}$$

where  $\sigma_{jb}^- = |j\rangle\langle b|$ ,  $\sigma_{j2}^- = |j\rangle\langle 2|$ ,  $\sigma_{01}^- = |1\rangle\langle 0|$ ,  $\sigma_{jj} = |j\rangle\langle j|$ ,  $\mathcal{L}[\Lambda] = \Lambda\rho\Lambda^+ - \Lambda^+\Lambda\rho/2 - \rho\Lambda^+\Lambda/2$  (with  $\Lambda = \hat{a}, \sigma_{jb}^-, \sigma_{j2}^-, \sigma_{01}^-$ ),  $\kappa$  is the decay rate of the cavity,  $\gamma_{jb}$  is the energy relaxation rate of the level  $|b\rangle$  for the decay path  $|b\rangle \rightarrow |j\rangle$  of the ququart ( $j = 0, 1, 2$ ),  $\gamma_{j2}$  ( $\gamma_{01}$ ) is the relaxation rate of the level  $|2\rangle$  for the decay path  $|2\rangle \rightarrow |j\rangle$  ( $|0\rangle \rightarrow |1\rangle$ ) of the ququart ( $j = 0, 1$ );  $\gamma_{j,\varphi}$  is the dephasing rate of the level  $|j\rangle$  of the ququart ( $j = 0, 2, b$ ).

The operational fidelity is given by  $F = \sqrt{\langle\psi_{\text{id}}|\rho|\psi_{\text{id}}\rangle}$ . Here,  $|\psi_{\text{id}}\rangle$  is the ideal output state of Eq. (13), which is achieved under the effective Hamiltonian (5) without taking into account the system dissipation and the unwanted couplings; while  $\rho$  is the density operator of the system for the operation being performed in a realistic situation.

The typical transition frequency between neighboring levels of a SC flux ququart can be made as 1 to 20 GHz [83-85]. As an example, we consider  $\omega_{1b}/2\pi = 14.5$  GHz,  $\omega_{2b}/2\pi = 12.5$  GHz,  $\omega_{0b}/2\pi = 13.5$  GHz,  $\omega_{12}/2\pi = 2.0$  GHz,  $\omega_{01}/2\pi = 1.0$  GHz, and  $\omega_c/2\pi = 10.5$  GHz. As a result, we have  $\Delta_{2b}/2\pi = 2.0$  GHz,  $\Delta_{1b}/2\pi = 4.0$  GHz,  $\Delta_{0b}/2\pi = 3.0$  GHz,  $\Delta_{01}/2\pi = -9.5$  GHz,  $\Delta_{02}/2\pi = -9.5$  GHz, and  $\Delta_{12}/2\pi = -8.5$  GHz. In addition, with appropriate design of the flux ququart [86], one can have  $\phi_{2b} \sim \phi_{1b} \sim \phi_{12} \sim 10\phi_{0b} \sim 10\phi_{02} \sim 10\phi_{01}$ , where  $\phi_{ij}$  represents the dipole coupling matrix element between the two levels  $|i\rangle$  and  $|j\rangle$ , with  $ij \in \{2b, 1b, 12, 0b, 02, 01\}$ . Since the coupling constant  $g_{ij}$  between the cavity and the  $|i\rangle \leftrightarrow |j\rangle$  transition of the ququart is proportional to the  $\phi_{ij}$  associated with the two

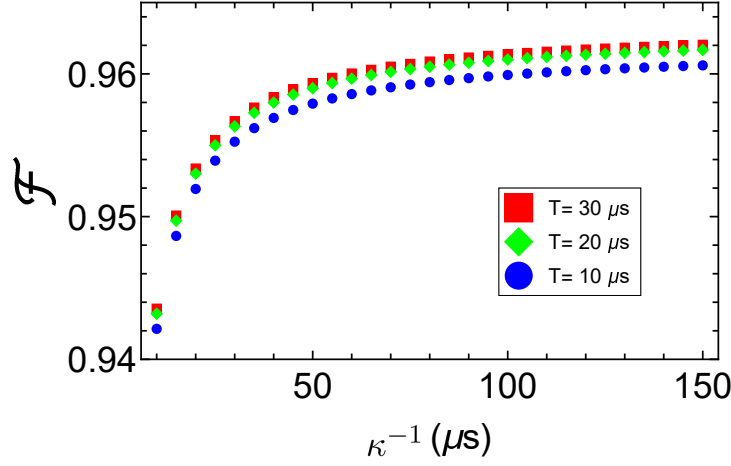


FIG. 3: (color online) Fidelity versus  $\kappa^{-1}$  for  $T = 10 \mu\text{s}$ ,  $20 \mu\text{s}$ , and  $30 \mu\text{s}$ .

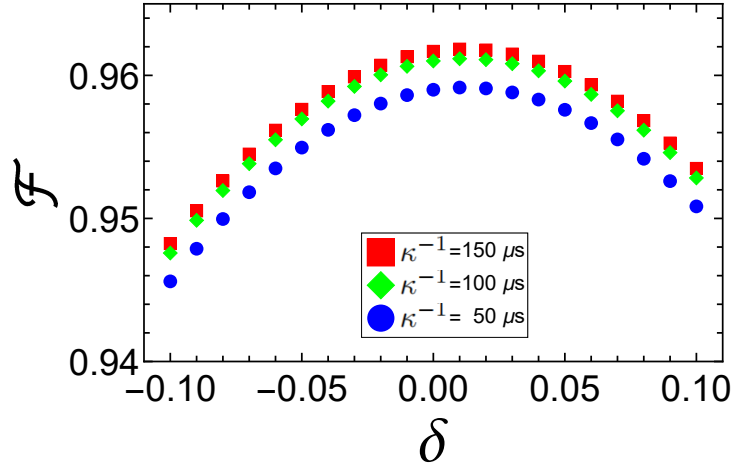


FIG. 4: (color online) Fidelity versus  $\delta$  for  $\kappa^{-1} = 50 \mu\text{s}$ ,  $100 \mu\text{s}$ , and  $150 \mu\text{s}$ . We set  $T = 20 \mu\text{s}$  in the numerical simulation.

levels  $|i\rangle$  and  $|j\rangle$ , one has  $g_{2b} \sim g_{1b} \sim g_{12} \sim 10g_{0b} \sim 10g_{02} \sim 10g_{01}$ . In the numerical simulations, we set  $g_{2b} = g_{1b} = g_{12} = 2\pi \times 120 \text{ MHz}$  and  $g_{0b} = g_{02} = g_{01} = 2\pi \times 12 \text{ MHz}$ , which are readily achievable in experiments [87].

Other parameters used in the numerical simulations are: (i)  $\gamma_{0b}^{-1} = \gamma_{02}^{-1} = \gamma_{01}^{-1} = 5T \mu\text{s}$ ,  $\gamma_{1b}^{-1} = \gamma_{2b}^{-1} = T/2 \mu\text{s}$ ,  $\gamma_{12}^{-1} = T \mu\text{s}$ , (ii)  $\gamma_{b,\phi}^{-1} = \gamma_{2,\phi}^{-1} = T/2 \mu\text{s}$ ,  $\gamma_{0,\phi}^{-1} = 2.5T$ , and (iii)  $\alpha = 3.05$ . For  $T = 20 \mu\text{s}$ , the decoherence times of the SC flux ququart used in the numerical simulations are  $10 \mu\text{s}$ – $100 \mu\text{s}$ , which is a rather conservative case as the decoherence time  $70 \mu\text{s}$  to  $1 \text{ ms}$  for a superconducting flux device has been experimentally demonstrated [52,88]. Furthermore, a cat state with  $\alpha = 3.05$  can be created in experiments because the circuit-QED experiments have generated a cat state with an amplitude  $\alpha \leq 5.27$  [78-82].

By numerically solving the master equation (15), Fig. 3 is plotted to show the fidelity versus  $\kappa^{-1}$  for  $T = 10 \mu\text{s}$ ,  $20 \mu\text{s}$ , and  $30 \mu\text{s}$ . Figure 3 shows that the fidelity exceeds 96.1% for  $\kappa^{-1} \geq 100 \mu\text{s}$  and  $T \geq 20 \mu\text{s}$ . Furthermore, Fig. 3 demonstrates that the fidelity is sensitive to the cavity decay and the decoherence of the ququart. This can be easily understood since the photons are populated in the cavity and both levels  $|0\rangle$  and  $|2\rangle$  of the ququart are occupied during the preparation of the hybrid entangled state (13).

In practice, the initial state of Eq. (12) may not be perfectly prepared. Thus, we consider a non-ideal initial state of the system

$$\begin{aligned}
 |\psi(0)\rangle_{\text{non-ideal}} &= \mathcal{N}_1^{-1} \left[ \left( \frac{1}{\sqrt{3}} + \delta \right) |0\rangle + \frac{1}{\sqrt{3}} |1\rangle + \left( \frac{1}{\sqrt{3}} - \delta \right) |2\rangle \right] \\
 &\quad \times \mathcal{N}_2 \left( \sqrt{1 + \delta} |\alpha\rangle + \sqrt{1 - \delta} |-\alpha\rangle \right),
 \end{aligned} \tag{16}$$

where  $\mathcal{N}_1 = \sqrt{1 + 2\delta^2}$  and  $\mathcal{N}_2 = 1/\sqrt{2 + 2\sqrt{1 - \delta^2}e^{-2|\alpha|^2}}$ . In this case, we numerically plot Fig. 4 for  $T = 20 \mu\text{s}$ .

Figure 4 shows that the fidelity decreases with increasing  $\delta$ . In addition, Fig. 4 shows that for  $\delta \in [-0.1, 0.1]$ , namely, a 10% error in the weights of  $|\alpha\rangle$  and  $|-\alpha\rangle$  states as well as in the weights of  $|0\rangle$  and  $|2\rangle$ , a fidelity greater than 94.5%, 94.7%, and 94.8% can be obtained for  $\kappa^{-1} = 50 \mu\text{s}$ ,  $100 \mu\text{s}$ ,  $150 \mu\text{s}$ , respectively.

The operational time for preparing the hybrid entangled state (13) is estimated to be  $\sim 0.046 \mu\text{s}$ , much shorter than the cavity decay time  $10 \mu\text{s}$ – $150 \mu\text{s}$  applied in the numerical simulations. For the cavity frequency given above and  $\kappa^{-1} = 100 \mu\text{s}$ , the quality factor of the cavity is  $Q \sim 6.59 \times 10^6$ , which is available because a 3D microwave cavity with a high quality factor  $Q = 3.5 \times 10^7$  was experimentally reported [89,90].

### C. Discussion

The above analysis shows that the operational fidelity is sensitive to errors in the initial state preparation, the cavity decay, and the decoherence of the SC ququart. Numerical simulations indicate that a high fidelity can still be obtained as long as the error in the initial state preparation is small. To obtain a high fidelity, it is necessary to reduce the error in the initial state prepare, select the cavity with a high quality factor, and use the SC ququart with a long coherence time. The fidelity can also be improved by employing the SC flux ququart with greater energy level anharmonicity, such that the unwanted couplings of the cavity with irrelevant level transitions of the SC flux ququart are negligible. Lastly, it should be remarked that further studies are needed for each particular experimental setup. However, this requires a rather lengthy and complex analysis, which is beyond the scope of this theoretical work.

## VI. CONCLUSIONS

We have proposed an approach to implement a hybrid two-qutrit CSUM gate with one SC qutrit controlling a target cat-state qutrit. The gate is realized by the dispersive coupling of the cavity to the SC ququart. As shown above, this proposal has the following features and advantages: (i) The gate realization is quite simple, because it requires only a single basic operation; (ii) Neither classical pulse nor measurement is needed; (iii) The hardware resources are minimized because no auxiliary system is required for the gate implementation; and (iv) The auxiliary higher energy level of the SC ququart is virtually excited during the gate operation, thus decoherence from this level is greatly suppressed. To our knowledge, this work is the first to demonstrate the realization of the proposed hybrid gate based on cavity or circuit QED. This proposal is quite general and can be applied to implement a hybrid two-qutrit CSUM gate with one matter qutrit (of different type) controlling a target cat-state qutrit in a wide range of physical system, such as a four-level natural atom or artificial atom (e.g., a quantum dot, an NV center, a SC ququart, etc.) coupled to an optical or microwave cavity.

As an application, we have further discussed the generation of a hybrid maximally-entangled state of a SC qutrit and a cat-state qutrit, by applying the proposed hybrid gate. To our knowledge, this work is the first to show the preparation of a hybrid entangled state of a SC qutrit and a cat-state qutrit. We have also numerically analyzed the experimental feasibility of generating such hybrid entangled state within current circuit QED technology. We hope that this work will stimulate experimental activities in the near future.

## ACKNOWLEDGEMENTS

This work was partly supported by the National Natural Science Foundation of China (NSFC) (11074062, 11374083, 11774076, U21A20436), the Jiangxi Natural Science Foundation (20192ACBL20051), and the Key-Area Research and Development Program of Guangdong province (2018B030326001).

- 
- [1] D. Deutsch, Quantum theory, the Church-Turing principle and the universal quantum computer, Proc. R. Soc. London, Ser. A **400**, 97 (1985); D. Deutsch, Quantum computational networks, Proc. R. Soc. London, Ser. A **425**, 73 (1989).
  - [2] P. W. Shor, in Proceedings of the 35th Annual Symposium on Foundations of Computer Science IEEE Computer Society Press, Santa Fe, NM, 1994.
  - [3] L. K. Grover, Quantum Mechanics Helps in Searching for a Needle in a Haystack, Phys. Rev. Lett. **79**, 325 (1997).
  - [4] T. C. Ralph, K. Resch, and A. Gilchrist, Efficient Toffoli gates using qudits, Phys. Rev. A **75**, 022313 (2007).
  - [5] D. Gottesman, in NASA International Conference on Quantum Computing and Quantum Communications (Springer, New York, 1998), pp. 302–313.
  - [6] Z. Gedik, I. A. Silva, B. Çakmak, G. Karpat, E. L. G. Vidoto, D. d. O. Soares-Pinto, E. Deazevedo, and F. F. Fanchini, Computational speed-up with a single qudit, Sci. Rep. **5**, 14671 (2015).
  - [7] S. S. Bullock, D. P. O’Leary, and G. K. Brennen, Asymptotically Optimal Quantum Circuits for d-Level Systems, Phys. Rev. Lett. **94**, 230502 (2005).



- [8] A. D. Greentree, S. G. Schirmer, F. Green, L. C. L. Hollenberg, A. R. Hamilton, and R. C. Clark, Maximizing the Hilbert Space for a finite number of distinguishable states, *Phys. Rev. Lett.* **92**, 097901 (2004).
- [9] H. H. Lu, Z. Hu, M. S. Alshaykh, A. J. Moore, Y. Wang, P. Imany, A. M. Weiner, and S. Kais, Quantum phase estimation with time-frequency qudits in a single photon, *Adv. Quantum Technol.* **3**, 1900074 (2019).
- [10] X. Gao, M. Erhard, A. Zeilinger, and M. Krenn, Computer-inspired concept for high-dimensional multipartite quantum gates, *Phys. Rev. Lett.* **125**, 050501 (2020).
- [11] A. B. Klimov, R. Guzmán, J. C. Retamal, and C. Saavedra, Qutrit quantum computer with trapped ions, *Phys. Rev. A* **67**, 062313 (2003).
- [12] S. D. Bartlett, H. de Guise, and B. C. Sanders, Quantum encodings in spin systems and harmonic oscillators, *Phys. Rev. A* **65**, 052316 (2002).
- [13] M. R. A. Adcock, P. Høyer, and B. C. Sanders, Quantum computation with coherent spin states and the close Hadamard problem, *Quantum Inf. Process.* **15**, 1361 (2016).
- [14] F. Dolde, V. Bergholm, Y. Wang, I. Jakobi, B. Naydenov, S. Pezzagna, J. Meijer, F. Jelezko, P. Neumann, T. Schulte-Herbruggen et al., High-fidelity spin entanglement using optimal control, *Nat. Commun.* **5**, 3371 (2014).
- [15] S. Dogra, Arvind, and K. Dorai, Determining the parity of a permutation using an experimental NMR qutrit, *Phys. Lett. A* **378**, 3452 (2014).
- [16] M. N. Leuenberger and D. Loss, Quantum computing in molecular magnets, *Nature (London)* **410**, 789 (2001).
- [17] R. Bianchetti, S. Filipp, M. Baur, J. M. Fink, C. Lang, L. Steffen, M. Boissonneault, A. Blais, and A. Wallraff, Control and Tomography of a Three Level Superconducting Artificial Atom, *Phys. Rev. Lett.* **105**, 223601 (2010).
- [18] M. A. Yurtalan, J. Shi, M. Kononenko, A. Lupascu, and S. Ashhab, Implementation of a Walsh-Hadamard gate in a superconducting qutrit, *Phys. Rev. Lett.* **125**, 180504 (2020).
- [19] A. Morvan, V. V. Ramasesh, M. S. Blok, J. M. Kreikebaum, K. O'Brien, L. Chen, B. K. Mitchell, R. K. Naik, D. I. Santiago, and I. Siddiqi, Qutrit Randomized Benchmarking, *Phys. Rev. Lett.* **126**, 210504 (2021).
- [20] M. S. Blok, V. V. Ramasesh, T. Schuster, K. O'Brien, J. M. Kreikebaum, D. Dahlen, A. Morvan, B. Yoshida, N. Y. Yao, and I. Siddiqi, Quantum Information Scrambling on a Superconducting Qutrit Processor, *Phys. Rev. X* **11**, 021010 (2021).
- [21] A. Cervera-Lierta, M. Krenn, Alán Aspuru-Guzik, and A. Galda, Experimental high-dimensional Greenberger-Horne-Zeilinger entanglement with superconducting transmon qutrits, arXiv:2104.05627
- [22] S. Muralidharan, C. L. Zou, L. Li, J. Wen, and L. Jiang, Overcoming erasure errors with multilevel systems, *New J. Phys.* **19**, 013026 (2017).
- [23] E. T. Campbell, Overcoming erasure errors with multilevel systems, *Phys. Rev. Lett.* **113**, 230501 (2014).
- [24] H. Bechmann-Pasquinucci and A. Peres, Quantum Cryptography with 3-State Systems, *Phys. Rev. Lett.* **85**, 3313 (2000).
- [25] D. Bruß and C. Macchiavello, Optimal Eavesdropping in Cryptography with Three-Dimensional Quantum States, *Phys. Rev. Lett.* **88**, 127901 (2002).
- [26] A. Vaziri, G. Weihs, and A. Zeilinger, Experimental Two-Photon, Three-Dimensional Entanglement for Quantum Communication, *Phys. Rev. Lett.* **89**, 240401 (2002).
- [27] R. Lapkiewicz, P. Li, C. Schaeff, N. K. Langford, S. Ramelow, M. Wieniak, and A. Zeilinger, Experimental non-classicality of an indivisible quantum system, *Nature (London)* **474**, 490 (2011).
- [28] A. Fedorov, L. Steffen, M. Baur, M. P. da Silva, and A. Wallraff, Implementation of a Toffoli gate with superconducting circuits, *Nature (London)* **481**, 170 (2012).
- [29] C. Song, S. B. Zheng, P. Zhang, K. Xu, L. Zhang, Q. Guo, W. Liu, D. Xu, H. Deng, K. Huang et al., Continuous-variable geometric phase and its manipulation for quantum computation in a superconducting circuit, *Nat. Commun.* **8**, 1061 (2017).
- [30] Y. H. Luo, H. S. Zhong, M. Erhard, X. L. Wang, L. C. Peng, M. Krenn, X. Jiang, L. Li, N. L. Liu, C. Y. Lu et al., Quantum Teleportation in High Dimensions, *Phys. Rev. Lett.* **123**, 070505 (2019).
- [31] X. M. Hu, C. Zhang, B. H. Liu, Y. Cai, X. J. Ye, Y. Guo, W. B. Xing, C. X. Huang, Y. F. Huang, C. F. Li et al., Experimental High-Dimensional Quantum Teleportation, *Phys. Rev. Lett.* **125**, 230501 (2020).
- [32] H. K. Xu, C. Song, W. Y. Liu, G. M. Xue, F. F. Su, H. Deng, Ye Tian, D. N. Zheng, S. Han, Y. P. Zhong et al., Coherent population transfer between uncoupled or weakly coupled states in ladder-type superconducting qutrits, *Nat. Commun.* **7**, 11018 (2016).
- [33] J. Daboul, X. Wang, and B. C. Sanders, Quantum gates on hybrid qudits, *J. Phys. A: Math. Gen.* **36**, 2525 (2003).
- [34] C. Bonato, F. Haupt, S. S. R. Oemrawsingh, J. Gudat, D. Ding, M. P. van Exter, and D. Bouwmeester, CNOT and Bell-state analysis in the weak-coupling cavity QED regime, *Phys. Rev. Lett.* **104**, 160503 (2010).
- [35] O. P. de SaNeto and M. C. de Oliveira, Quantum bit encoding and information processing with field superposition states in a circuit, *J. Phys. B* **45**, 185505 (2012).
- [36] J. D. Pritchard, J. A. Isaacs, M. A. Beck, R. McDermott, and M. Saffman, Hybrid atom-photon quantum gate in a superconducting microwave resonator, *Phys. Rev. A* **89**, 010301(R) (2014).
- [37] H. R. Wei and G. L. Long, Hybrid quantum gates between flying photon and diamond nitrogen-vacancy centers assisted by optical microcavities, *Sci. Rep.* **5**, 12918 (2015).
- [38] D. Yu, M. M. Valado, C. Hufnagel, L. C. Kwek, L. Amico, and R. Dumke, Charge-qubit-atom hybrid, *Phys. Rev. A* **93**, 042329 (2016).
- [39] B. C. Ren and F. G. Deng, Robust hyperparallel photonic quantum entangling gate with cavity QED, *Opt. Express* **25**, 10863 (2017).
- [40] D. Kim and K. Moon, Hybrid two-qubit gate using circuit QED system with triple-leg stripline resonator, arXiv:1808.02865.
- [41] C. P. Yang, Z. F. Zheng, and Y. Zhang, Universal quantum gate with hybrid qubits in circuit quantum electrodynamics,

- Opt. Lett. **43**, 5765 (2018).
- [42] Y. B. Liu, L. Li, and Y. Q. Ma, A Hybrid Rydberg Quantum Gate for Quantum Network, arXiv:2105.00289.
- [43] G. Z. Song, J. L. Guo, Q. Liu, H. R. Wei, and G. L. Long, Heralded quantum gates for hybrid systems via waveguide-mediated photon scattering, Phys. Rev. A **104**, 012608 (2021).
- [44] C. P. Yang, S. I. Chu, and S. Han, Possible realization of entanglement, logical gates, and quantum information transfer with superconducting-quantum-interference-device qubits in cavity QED, Phys. Rev. A **67**, 042311 (2003).
- [45] J. Q. You and F. Nori, Quantum information processing with superconducting qubits in a microwave field, Phys. Rev. B **68**, 064509 (2003).
- [46] A. Blais, R. S. Huang, A. Wallraff, S. M. Girvin, and R. J. Schoelkopf, Cavity quantum electrodynamics for superconducting electrical circuits: An architecture for quantum computation, Phys. Rev. A **69**, 062320 (2004).
- [47] J. Q. You and F. Nori, Atomic physics and quantum optics using superconducting circuits, Nature (London) **474**, 589 (2011).
- [48] Z. L. Xiang, S. Ashhab, J. Q. You, and F. Nori, Hybrid quantum circuits: Superconducting circuits interacting with other quantum systems, Rev. Mod. Phys. **85**, 623 (2013).
- [49] X. Gu, A. F. Kockum, A. Miranowicz, Y. X. Liu, and F. Nori, Microwave photonics with superconducting quantum circuits, Phys. Rep. **718**, 1 (2017).
- [50] P. B. Li, Y. C. Liu, S. Y. Gao, Z. L. Xiang, P. Rabl, Y. F. Xiao, and F. L. Li, Hybrid quantum device based on NV centers in diamond nanomechanical resonators plus superconducting waveguide cavities. Phys. Rev. Appl. **4**, 044003 (2015).
- [51] J. Joo, C. W. Lee, S. Kono, and J. Kim, Logical measurement-based quantum computation in circuit QED, Sci. Rep. **9**(1), 16592 (2019).
- [52] F. Yan, S. Gustavsson, A. Kamal, J. Birenbaum, A. P. Sears, D. Hover, T. J. Gudmundsen, J. L. Yoder, T. P. Orlando, J. Clarke et al., The Flux Qubit Revisited to Enhance Coherence and Reproducibility, Nat. Commun. **7**, 12964 (2016).
- [53] A. P. M. Place, L. V. H. Rodgers, P. Mundada, B. M. Smitham, M. Fitzpatrick, Z. Leng, A. Premkumar, J. Bryon, A. Vrajitoarea, S. Sussman et al., New material platform for superconducting transmon qubits with coherence times exceeding 0.3 milliseconds, Nat. Commun. **12**, 1779 (2021).
- [54] C. L. Wang, X. G. Li, H. K. Xu, Z. Y. Li, J. H. Wang, Z. Yang, Z. Y. Mi, X. H. Liang, T. Su, C. H. Yang et al., Transmon qubit with relaxation time exceeding 0.5 milliseconds, arXiv:2105.09890.
- [55] A. Somoroff, Q. Ficheux, R. A. Mencia, H. N. Xiong, R. Kuzmin, and V. E. Manucharyan, Millisecond coherence in a superconducting qubit, arXiv:2103.08578.
- [56] Z. Leghtas, G. Kirchmair, B. Vlastakis, R. J. Schoelkopf, M. H. Devoret, and M. Mirrahimi, Hardware-Efficient Autonomous Quantum Memory Protection, Phys. Rev. Lett. **111**, 120501 (2013).
- [57] M. Mirrahimi, Z. Leghtas, V. V. Albert, S. Touzard, R. J. Schoelkopf, L. Jiang, and M. H. Devoret, Dynamically protected cat-qubits: a new paradigm for universal quantum computation, New J. Phys. **16**, 045014 (2014).
- [58] V. V. Albert, C. Shu, S. Krastanov, C. Shen, R.-B. Liu, Z.-B. Yang, R. J. Schoelkopf, M. Mirrahimi, M. H. Devoret, and L. Jiang, Holonomic quantum control with continuous variable systems, Phys. Rev. Lett. **116**, 140502 (2016).
- [59] J. Guillaud and M. Mirrahimi, Repetition cat qubits for fault-tolerant quantum computation, Phys. Rev. X **9**, 041053 (2019).
- [60] C. Chamberland, K. Noh, P. Arrangoiz-Arriola, E. T. Campbell, C. T. Hann, J. Iverson, H. Putterman, T. C. Bohdanowicz, S. T. Flammia, A. Keller et al., Building a fault-tolerant quantum computer using concatenated cat codes, arXiv:2012.04108.
- [61] É. Gouzien and N. Sangouard, Factoring 2048-bit RSA Integers in 177 Days with 13 436 Qubits and a Multimode Memory, Phys. Rev. Lett. **127**, 140503 (2021).
- [62] N. Ofek, A. Petrenko, R. Heeres, P. Reinhold, Z. Leghtas, B. Vlastakis, Y. Liu, L. Frunzio, S. M. Girvin, L. Jiang et al., Extending the lifetime of a quantum bit with error correction in superconducting circuits, Nature (London) **536**, 441 (2016).
- [63] Y. Wang, Z. Hu, B. C. Sanders, and S. Kais, Qudits and high-dimensional quantum computing, Front. Phys. **8**, 479 (2020).
- [64] Sean Clark, Valence bond solid formalism for d-level one-way quantum computation, J. Phys. A: Math. Gen. **39**, 2701 (2006).
- [65] J. L. Brylinski and R. Brylinski, Universal quantum gates, arXiv:quant-ph/0108062
- [66] S. B. Zheng and G. C. Guo, Efficient Scheme for Two-Atom Entanglement and Quantum Information Processing in Cavity QED, Phys. Rev. Lett. **85**, 2392 (2000).
- [67] A. Sorensen and K. Molmer, Quantum Computation with Ions in Thermal Motion, Phys. Rev. Lett. **82**, 1971 (1999).
- [68] D. F. V. James, and J. Jerke, Effective Hamiltonian theory and its applications in quantum information, Can. J. Phys. **85**, 625 (2007).
- [69] M. Neeley, M. Ansmann, R. C. Bialczak, M. Hofheinz, N. Katz, E. Lucero, A. O'Connell, H. Wang, A. N. Cleland, and J. M. Martinis, Process tomography of quantum memory in a Josephson-phase qubit coupled to a two-level state, Nat. Phys. **4**, 523 (2008).
- [70] G. Sun, X. Wen, B. Mao, J. Chen, Y. Yu, P. Wu, and S. Han, Tunable quantum beam splitters for coherent manipulation of a solid-state tripartite qubit system, Nat. Commun. **1**, 51 (2010).
- [71] R. Barends, J. Kelly, A. Megrant, A. Veitia, D. Sank, E. Jeffrey, T. C. White, J. Mutus, A. G. Fowler, B. Campbell et al., Superconducting quantum circuits at the surface code threshold for fault tolerance, Nature (London) **508**, 500 (2014).
- [72] M. Sandberg, C. M. Wilson, F. Persson, T. Bauch, G. Johansson, V. Shumeiko, T. Duty, and P. Delsing, Tuning the field in a microwave resonator faster than the photon lifetime, Appl. Phys. Lett. **92**, 203501 (2008).
- [73] Z. L. Wang, Y. P. Zhong, L. J. He, H. Wang, J. M. Martinis, A. N. Cleland, and Q. W. Xie, Quantum state characterization

- of a fast tunable superconducting resonator, *Appl. Phys. Lett.* **102**, 163503 (2013).
- [74] M. Silva and C. R. Myers, Computation with coherent states via teleportations to and from a quantum bus, *Phys. Rev. A* **78**, 062314 (2008).
- [75] L. P. van, Optical hybrid approaches to quantum information, *Laser Photonics Rev.* **5**, 167 (2011).
- [76] U. L. Andersen, J. S. Neergaard-Nielsen, L. P. van, and A. Furusawa, Hybrid quantum information processing, *Nat. Phys.* **11**, 713 (2015).
- [77] B. Ye, Z. F. Zheng, and C. P. Yang, Multiplex-controlled phase gate with qubits distributed in a multicavity system, *Phys. Rev. A* **97**, 062336 (2018).
- [78] A. Grimm, N. E. Frattini, S. Puri, S. O. Mundhada, S. Touzard, M. Mirrahimi, S. M. Girvin, S. Shankar, and M. H. Devoret, Stabilization and operation of a Kerr-cat qubit, *Nature (London)* **584**, 205 (2020).
- [79] G. Kirchmair, B. Vlastakis, Z. Leghtas, S. E. Nigg, H. Paik, E. Ginossar, M. Mirrahimi, L. Frunzio, S. M. Girvin, and R. J. Schoelkopf, Observation of quantum state collapse and revival due to the singlephoton Kerr effect, *Nature (London)* **495**, 205 (2013).
- [80] B. Vlastakis, G. Kirchmair, Z. Leghtas, S. E. Nigg, L. Frunzio, S. M. Girvin, M. Mirrahimi, M. H. Devoret, and R. J. Schoelkopf, Deterministically encoding quantum information using 100-photon Schrodinger cat states, *Science* **342**, 607 (2013).
- [81] L. Sun, A. Petrenko, Z. Leghtas, B. Vlastakis, G. Kirchmair, K. M. Sliwa, A. Narla, M. Hatridge, S. Shankar, J. Blumoff et al., Tracking photon jumps with repeated quantum non-demolition parity measurements, *Nature (London)* **511**, 444 (2014).
- [82] B. Vlastakis, A. Petrenko, N. Ofek, L. Sun, Z. Leghtas, K. Sliwa, Y. Liu, M. Hatridge, J. Blumoff, L. Frunzio et al., Characterizing entanglement of an artificial atom and a cavity cat state with Bell's inequality, *Nat. Commun.* **6**, 8970 (2015).
- [83] A. O. Niskanen, K. Harrabi, F. Yoshihara, Y. Nakamura, S. Lloyd, and J. S. Tsai, Quantum Coherent Tunable Coupling of Superconducting Qubits, *Science* **316**, 723 (2007).
- [84] K. Inomata, T. Yamamoto, P. M. Billangeon, Y. Nakamura, and J. S. Tsai, Large dispersive shift of cavity resonance induced by a superconducting flux qubit in the straddling regime, *Phys. Rev. B* **86**, 140508 (2012).
- [85] Z. H. Peng, Y. X. Liu, J. T. Peltonen, T. Yamamoto, J. S. Tsai, and O. Astafiev, Correlated Emission Lasing in Harmonic Oscillators Coupled via a Single Three-Level Artificial Atom, *Phys. Rev. Lett.* **115**, 223603 (2015).
- [86] Y. X. Liu, J. Q. You, L. F. Wei, C. P. Sun, and F. Nori, Optical selection rules and phase dependent adiabatic state control in a superconducting quantum circuit, *Phys. Rev. Lett.* **95**, 087001 (2005).
- [87] T. Niemczyk, F. Deppe, H. Huebl, E. P. Menzel, F. Hocke, M. J. Schwarz, J. J. Garcia-Ripoll, D. Zueco, T. Hummer, E. Solano, A. Marx, and R. Gross, Circuit quantum electrodynamics in the ultrastrong coupling regime, *Nat. Phys.* **6**, 772 (2010).
- [88] J. Q. You, X. Hu, S. Ashhab, and F. Nori, Low-decoherence flux qubit, *Phys. Rev. B* **75**, 140515 (2007).
- [89] C. Wang, Y. Y. Gao, P. Reinhold, R. W. Heeres, N. Ofek, K. Chou, C. Axline, M. Reagor, J. Blumoff, K. M. Sliwa et al., A Schrodinger cat living in two boxes, *Science* **352**, 1087 (2016).
- [90] M. Reagor, W. Pfaff, C. Axline, R. W. Heeres, N. Ofek, K. Sliwa, E. Holland, C. Wang, J. Blumoff, K. Chou et al., A quantum memory with near-millisecond coherence in circuit QED, *Phys. Rev. B* **94**, 014506 (2016).